Title

Geographic Atrophy: Confocal Scanning Laser Ophthalmoscopy, Histology, and Inflammation in the Region of Expanding Lesions

Journal

Investigative Ophthalmology & Visual Science, 61(8)

ISSN

0146-0404

Authors

Bonilha, Vera L
Bell, Brent A
Hu, Jane
et al.

Publication Date

2020-07-13

DOI

10.1167/iovs.61.8.15

Peer reviewed

Geographic Atrophy: Confocal Scanning Laser Ophthalmoscopy, Histology, and Inflammation in the Region of Expanding Lesions

Vera L. Bonilha,[1,2] Brent A. Bell,[1,*] Jane Hu,[3] Caroline Milliner,[1] Gayle J. Pauer,[1] Stephanie A. Hagstrom,[1,2] Roxana A. Radu,[3] and Joe G. Hollyfield[1,2]

[1]Cole Eye Institute, Cleveland Clinic, Cleveland, Ohio, United States
[2]Department of Ophthalmology, Cleveland Clinic Lerner College of Medicine of Case Western Reserve University, Cleveland, Ohio, United States
[3]UCLA Stein Eye Institute and Department of Ophthalmology, David Geffen School of Medicine, University of California at Los Angeles, Los Angeles, California, United States

Correspondence: Vera L. Bonilha, Ophthalmic Research–i31, Cole Eye Institute, Cleveland Clinic, 9500 Euclid Avenue, Cleveland, OH 44195, USA;
bonilhav@ccf.org.

Current affiliation: *Scheie Eye Institute, University of Pennsylvania, Philadelphia, Pennsylvania, United States.

Received: November 8, 2019
Accepted: May 8, 2020
Published: July 13, 2020

Citation: Bonilha VL, Bell BA, Hu J, et al. Geographic atrophy: Confocal scanning laser ophthalmoscopy, histology, and inflammation in the region of expanding lesions. *Invest Ophthalmol Vis Sci.* 2020;61(8):15. https://doi.org/10.1167/iovs.61.8.15

Purpose. To describe the pathology of AMD in eyes with geographic atrophy (GA) using confocal scanning laser ophthalmoscopy (SLO) blue light autofluorescence (BAF), and near-infrared (IR) AF and to correlate it with the histology and immunohistochemistry analysis at the margins of the GA lesion.

Methods. Enucleated, fixed eyes from seventeen donors with GA were imaged and analyzed by BAF-SLO, IRAF-SLO, and by fundus macroscopy (FM). Tissue from the margins of the GA lesions was cut and processed for resin embedding and histology or cryosectioning and fluorescence in the green and far-red channels, and immunohistochemistry to assess markers of inflammation. Isolated DNA from donors was genotyped for single nucleotide polymorphisms (SNPs) previously shown to be risk factors for the development and progression of AMD.

Results. Around the leading edge of the GA lesions we observed hypertrophic RPE cells with cytoplasm filled with granules fluorescent both in the far-red and green-red channels; abundant microglia and macrophage; deposition of complement factor H (CFH) in Bruch's membrane (BM) and increased membrane attack complex (MAC) on RPE cells.

Conclusions. Fluorescence imaging of cryosections of RPE cells around the leading edge of the GA lesions suggest that IRAF-SLO visualizes mostly melanin-related compounds. In addition, medium-size GA atrophy displayed the most significant changes in inflammation markers.

Keywords: age-related macular degeneration, confocal scanning laser ophthalmoscopy, autofluorescence, histology, inflammation

Age-related macular degeneration (AMD) is the most common cause of irreversible blindness in the elderly population of industrialized countries. AMD occurs in two forms: neovascular (wet) and nonneovascular (dry). Wet AMD is characterized by abnormal capillary growth originating from the choroid into Bruch's membrane (BM) and RPE, or from retina followed by disruption of outer retinal layers with subsequent exudation of fluid, lipid, and blood. Dry AMD is characterized by the early degeneration of the choriocapillaris and the focal and progressive atrophy of the RPE, followed by photoreceptor cell loss in and around the foveal region. This form of macular degeneration is also referred to as *geographic atrophy* (GA).

Lipofuscin is a long-lived intracellular inclusion body, lipid- and bisretinoids-rich, autofluorescent material that progressively accumulates in the RPE.[1–3] In the early stages of AMD, lipofuscin amasses within the RPE cytoplasm and exerts a cytotoxic effect related to the pathology of GA by means of mechanical distortions of cellular architecture and by enhancing phototoxicity.[4–6] The RPE lipofuscin accumulation can be visualized in patients using the blue peak (BAF-SLO) autofluorescence (AF) mode from a confocal scanning laser ophthalmoscope (SLO).[7] Previous studies involving BAF-SLO imaging documented GA growth rates for a number of GA lesions.[8] Another report identified increased, but irregular AF patterns in the junctional zone of GA.[9] Importantly, quantification of GA lesion size using BAF-SLO imaging is the primary outcome measure in various ongoing clinical trials investigating GA[10] (NCT02247531, NCT02247479, NCT02087085; http://clinicaltrials.gov). Recent research suggested that RPE dysmorphia such as rounding and stacking of the RPE may explain the variable AF in the leading-edge areas of the GA atrophy.[11] At the cellular level, a recent study reported that intracellular aggregation of lipofuscin and melanolipofuscin

granules were observed exclusively in AMD eyes including eyes with GA.[5]

Near-infrared SLO autofluorescence (IRAF-SLO) is yet another SLO modality that has been used in recent years to document invisible, far-red fluorescence originating from the posterior pole. More specifically, this mode has been useful for ascertaining melanin and its related compounds (melanolipofuscin, melanolysosomes, and oxidized melanin) residing within the RPE cells and choroid.[12,13] However, to our knowledge, a comparison between histopathologic and IRAF-SLO findings in AMD and control RPE has not been reported. In this study, we characterized the RPE, and the autofluorescent granules present in the leading-edge of the GA using filters similar in excitation and emission wavelength ranges as those used by BAF- and IRAF-SLO imaging modalities in the ophthalmology clinics.

Recent studies have indicated that several proteins associated with the immune system, such as C3, C5b–C9 (membrane attack complex, MAC), and CFH, are present in high quantity in the BM and drusen in AMD.[14–16] Also, recruitment of microglia/monocytes in the macula region of all forms of AMD pathology have been reported.[17] These observations underline the potential importance of a disordered immune system in AMD.

Here, we report the correlation of ex vivo imaging in fixed globes with ocular histopathology from AMD donors with GA. Specifically, we characterize and quantify the GA lesion, and the RPE and retinal pathology present within the GA border. Our data support the loss of RPE cell polarity around the leading edge of the GA lesions, with the presence of hypertrophic RPE cells with their cytoplasm filled with granules fluorescent both in the green-red and far-red channels. Moreover, we identified the presence of pigmented granules localized to the apical surface of the RPE cells from both control and AMD donors in regions outside of the GA lesions. These granules did not fluoresce in any of the wavelengths investigated. Finally, we identified the increased presence of microglia and macrophage, and amplified deposition of CFH in BM, and MAC of RPE within the GA border.

Methods

Tissue Acquisition and Fixation

Donor eyes were obtained through the Foundation Fighting Blindness (FFB) Eye Donor Program (Columbia, MD, USA). Eye bank records accompanying the donor eyes indicated whether the donor had AMD or no known eye diseases. Pathology was individually assessed by fundus macrophotography (FM) on receipt. Immunohistochemical analysis was performed with the approval of the Cleveland Clinic Institutional Review Board (IRB no. 14-057). The research adhered to the tenets of the Declaration of Helsinki. Tissue from 32 AMD donor eyes from 17 donors was analyzed; their ages varied between 65 and 97, and the interval between death and tissue processing varied between three and 33 hours. Controls included 10 postmortem eyes from 10 donors (one eye per donor) without any history of ocular disease, and confirmed to be free of macular lesions via FM assessment. Additional information about the donors is provided in Table 1. Globes were fixed and shipped from the eye banks to our lab in 4% paraformaldehyde and 0.5% glutaraldehyde made in Dulbecco's phosphate buffered saline (D-PBS) buffer. On receiving, globes were cut through the ora serrata, imaged by FM submerged in D-PBS, and stored in 2% paraformaldehyde made in D-PBS.

Genetic Analysis

DNA was extracted from blood or eye tissue using the Gentra Puregene Blood Kit (QIAGEN, Germantown, MD, USA). Samples were genotyped using TaqMan SNP genotyping assays. Donor samples were genotyped for single nucleotide polymorphisms (SNPs) correlated with AMD (rs1061170 (*CFH*), rs10490924 (*ARMS2*), rs11200638 (*HTRA1*), and rs2230199 (*C3*)[18] and for SNPs previously shown to be associated with GA (rs2842992, near SOD2; rs1789110, near MBP; rs722782, near C80rf42).[19]

Ex Vivo Imaging of Eyes

Posterior poles were transferred to a chamber filled with D-PBS solution and imaged as previously described.[20] Briefly, FM images were collected using a Zeiss AxioCam MRC5 camera equipped with a macro zoom lens and AxioVision AC Software (Zeiss, Oberkochen, Germany). SLO images were collected using a HRA2 confocal scanning laser ophthalmoscope (Heidelberg Engineering, Inc., Heidelberg, Germany). Quantification of the diameter of the GA lesions was calculated using the SLO images calibrated to a 1-mm ruby sphere (Edmund Optics, Inc, Barrington, NJ, USA) placed on the optic nerve head and delineated using the freehand line tool in ImageJ2 software.

Histology and Ultrastructural Analysis

Isolated fragments of retina-RPE-choroid in the edge of the GA lesion were cut from the following regions: superior (region 1), temporal (region 2), inferior (region 3), and nasal (region 4) as shown in Figure 2A (white rectangles). Tissue was further fixed by immersion in 2.5% glutaraldehyde in 0.1M cacodylate buffer, post-fixed with 1% osmium tetroxide for 45 minutes on ice, sequentially dehydrated in ethanol, and embedded in Epon as previously described.[20] Toluidine blue–stained sections were photographed with a Zeiss AxioImager.Z1 light microscope using a ×20, numerical aperture 0.5 plan neofluar objective (Zeiss, 440340) and analyzed for occurring frequencies of existence of RPE cells within 400 µm of the edge of the GA lesion. Statistical analysis was performed as described below. Ultrathin sections were prepared, and electron micrographs were taken on a Tecnai G2 SpiritBT operated at 80 kV (FEI Company, Hillsboro, OR, USA) and on a JEM 1200-EX electron microscope (JEOL, Peabody, MA, USA).

Autofluorescence of Unlabeled Cryosections

Isolated fragments of retina-RPE-choroid were placed in 4% paraformaldehyde in D-PBS, followed by changes to 10% (1h) and 20% sucrose (overnight) made in D-PBS and finally a mix of 20% sucrose and Tissue-Tek "4583" (Miles Inc.). Cryosections (10 µm) were imaged using brightfield and epifluorescence using filters that mimicked the HRA2 BAF and IRAF-SLO: green/red (excitation 480 nm/emission >500–680 nm) and far-red channels (excitation 750 nm/emission >800 nm) with a Zeiss AxioImager.Z1 light microscope using a ×40, numerical aperture 1.3 plan neofluar oil immersion objective (Zeiss, 440456, Raleigh

Investigative Ophthalmology & Visual Science

Table 1. AMD Human Donor Additional Information

Donor ID	Age[*]	Sex	Race	D-to-P[†]	Ocular History[‡]
1	90	M	C	16	Neovascular AMD
2	87	F	C	5	Nonneovascular AMD
3	95	F	C	7	AMD
4	94	M	C	6	AMD
5	96	F	C	9	AMD
6	91	F	C	15	AMD
7	90	F	C	15	AMD
8	87	M	C	12	Nonneovascular AMD
9	94	F	C	21	AMD
10	87	F	C	11	AMD
11	87	F	C	33	Nonneovascular AMD
12	97	F	C	5	Neovascular AMD
13	86	F	C	23	Neovascular (exudative)[§] AMD
14	86	F	C	9.4	AMD (neovascular & nonneovascular)
15	85	F	C	8	AMD (neovascular – exudative - OD[‖] & nonneovascular)
16	89	F	C	9	AMD
17	65	M	C	18.5	AMD
C1	92	M	C	11	None
C2	84	F	C	10	None
C3	66	F	C	6	None
C4	72	M	C	5.8	None
C5	91	M	C	8	None
C6	95	F	C	4	None
C7	57	F	C	13	None
C8	78	M	C	4.5	None
C9	66	F	C	8	None
C10	71	F	C	7	None

M, male; F, female; C, Caucasian.
[*] Age at death (years).
[†] Interval from death to preservation (hours).
[‡] Ocular Disease Classification according to both eye bank records and fundus imaging.
[§] Donor was treated with Avastin for three years according to the eye bank record.
[‖] Eye bank record indicated that donor received "injections" in the right eye.

formula theoretical resolutions of 0.23 & 0.35 µm at 480 nm and 750 nm, respectively) and a Zeiss apotome. Serial Z-stacks were acquired through the cryosections. Images were collected in sequence on an Axiocam 503 mono camera (Carl Zeiss Microscopy, LLC, Thornwood, NY, USA) using exposures of 7 ms (brightfield), 88 ms (green/red channel), and 14 s (far-red channel). The frequency of lipofuscin, melanosomes, and melanolipofuscin granules was quantified within 200 µm of the edge of the GA lesion using ImageJ2 software. Micrographs were calibrated from a reference scale embedded in the image using the Zeiss AxioImager software. Automatic particle counting was performed after images were converted into a binary (black and white) image and the threshold range was set to highlight as many individual granules as possible, as described in the ImageJ manual. Granules not counted automatically were manually counted using the Point Picker tool or "Cell counter" plugin to correct and complete the quantification as needed.

Histopathology of Inflammation Markers

Cryosections were blocked in PBS supplemented with 1% BSA (PBS/BSA) for 30 min and incubated with the following antibodies: Iba-1 (019-19741, rabbit IgG, 1:250, Wako Chemicals USA, Inc., Richmond, VA, USA) and CD68 (MA5-13324, mouse IgG1, 1:20; Thermofisher, Waltham, MA, USA), in 1% PBS/BSA overnight at 4°C. Parallel sections were treated with the Delicate Melanin Bleach Kit (24909, Polysciences, Inc, Warrington, PA, USA) according to the manufacturer's instruction before incubation with an antibody to human CFH (A312, 1:250; Quidel, San Diego, CA, USA), and C5b-9 (M0777, 1:50; Dako, Glostrup, Denmark). Sections were then labeled with secondary antibodies conjugated with Alexa Fluor 488 and 594 (Molecular Probes, 1:1000) for 45 min. at room temperature. Cell nuclei were labeled with TO-PRO-3 iodide (Thermofisher). Images were acquired using a Leica laser scanning confocal microscope (TCS-SP8; Leica, Exton, PA, USA) with a series of 0.33µm xy (en face) optical sections using a ×40, numerical aperture 1.3 HC PL APO CS2 oil immersion objective (Leica, 11506358). Each individual xy image of the stained retinas represents a three-dimensional projection of the entire cryosection (Z-stack sum). Micrograph panels were composed using AdobePhotoshop CC (Adobe, San Jose, CA, USA). The GA border was defined by the descent of the external limiting membrane (ELM) toward the BM, as previously reported.[11] Quantification of complement protein immunoreactivity signal intensity and Iba-1+ cells was performed using ImageJ2 software. Micrographs were calibrated using a scale embedded in the image. The signal intensity through the whole retina was quantified within 0 to 200 µm, and 200 to 400 µm of the edge of the GA lesion and the corrected total cell fluorescence (CTCF) was

Investigative Ophthalmology & Visual Science

calculated for each area according to the following formula: CTCF = Integrated Density – (Area of selected cell × Mean fluorescence of background readings). Frequency of Iba-1 + cells was quantified using ImageJ Point Picker or "Cell counter" plugins.

Statistics

All data were analyzed using GraphPad Prism v8.1.1 (GraphPad Software, La Jolla, CA, USA). All data are presented as mean± SEM. Two-way analysis of variance with Turkey's multiple comparisons test was used for determining statistical significance with an alpha value of 0.05.

Results

Molecular Genetic Analysis

Thirty-four donor eyes with GA and 10 age-matched, non-AMD (control) eyes were evaluated for eight SNPs previously associated with the risk and progression of AMD and GA. The identified SNPs for each donor are shown in Table 2. No specific association of any of the SNPs analyzed in donor eyes with GA was identified.

Ex Vivo Imaging of Donor Eyes

Gross pathology of donor eyes was first assessed by FM (Figs. 1A–1G), BAF-SLO (Figs. 1H–1N), and IRAF-SLO images (Figs. 1O–1U). Anatomic landmarks, such as the optic disk (Fig. 1, ON) and fovea (Figs. 1A–1G, arrow), are identifiable in the control example 92-year-old (Fig. 1A) and in several of GA eyes by fundus microscopy (Figs. 1B–1G). The GA is visible in all three imaging modalities. In the majority of GA eyes (Figs. 1C–1G), RPE atrophy is delineated (arrowheads) with blood vessels (Fig. 1, asterisk) frequently visible because of RPE atrophy and loss of melanin pigment. However, in the donor 7 eye (Fig. 1B), the GA boundary was difficult to discern by fundus imaging. Visualization of donor eyes in BAF-SLO modality (Figs. 1H–1N) did not result in images with well-defined or easily discerned atrophic borders possibly due to reduced optical transparency of inner retina observed in post-mortem samples. In contrast, visualization by IRAF-SLO (Figs. 1O–1U) did result in visible, well-defined atrophic borders for the majority of AMD donor eyes that can be attributed to reduced optical scattering commonly observed for near IR versus the shorter visible light wavelengths. Because of the enhanced clarity of IRAF-SLO over BAF-SLO, we used the former to quantify the area of each GA lesion using a ruby sphere of known size (Table 2). Previous studies assessing GA progression reported that areas of GA lesions continue to enlarge over time and result in a significant decline in visual acuity accompanied by disease severity.[21,22] Thus, for analysis purpose, we elected to segregate our GA findings into three groups that included donors with small (<1.1 mm^2), medium (1.1–3.0 mm^2) and large (>3.1 mm^2) areas of atrophy. In donor eyes with large areas of atrophy BAF-SLO imaging detected patchy, circumferentially discontinuous areas of increased AF along the outside rim of the GA area (Figs. 1M, 1N). Foveal sparing was mostly noted with fundus macroscopy (Figs. 1B–1G, arrow) and BAF-SLO (Figs. 1I–1N, arrow) but not IRAF-SLO.

Histopathology at the Border of the GA Lesion

A schematic overlay depicts the regions harvested and processed for observation in both the histological, autofluorescence and immunohistologic assays (Fig. 2A, white rectangles). Histology of the control retinas typically displayed normal retinal lamination (Fig. 2B). Their RPE displayed slightly "nonuniform" morphology and pigment distribution with basal laminar deposit (Fig. 2B, BLamD) over the BM. In all of the GA donors, the descent of the external limiting membrane (ELM, yellow arrowheads) toward BM was evident at the edge of the atrophy (Figs. 2C–2G), as previously reported in histologic sections and OCT imaging.[11,23] The edge of the GA lesion in AMD donors displayed a few degenerated cone photoreceptor cell bodies lacking outer segments (Figs 2C–2G). RPE morphology within the GA border included several of the RPE phenotypes, recently described to explain various RPE pathways in AMD pathogenesis,[24] including very nonuniform RPE (Fig. 2C), dissociated RPE (Fig. 2D), bilaminar RPE (Fig. 2F), shedding RPE (Fig. 2E), sloughed RPE (Fig. 2G). The frequency of the RPE morphology observed at the edge of the GA in AMD donors is summarized in Table 3: most frequent types of RPE phenotypes were very nonuniform (48.84 %), dissociated (37.21 %), and sloughed (32.56 %) cells.

Distribution of Autofluorescent Granules at the Border of GA

Clinical imaging of the eye with SLO aims to document the RPE lipofuscin fluorophores and melanin. It facilitates the diagnosis and evaluation of treatment response. We aimed to document the cellular distribution of these autofluorescent materials in the RPE at the border of GA by fluorescence microscopy using excitation/emission paradigms that match the Heidelberg Engineering SLO imaging system. The RPE situated at the border of the GA lesion displayed apical dark-pigments that did not fluoresce with either the green/red (Fig. 3A) or far-red channels (Fig. 3B, white arrowheads). A similar pattern of distribution was also observed in the RPE from non-AMD, age-matched control donor eyes (Supplementary Figs. S1G, S1H). At the GA border (Figs. 3C–3L), the AMD donor eyes displayed hypertrophic RPE cells with cytoplasm filled with fluorescent granules in both the green/red (Figs. 3C, 3E, 3G, 3I, and 3K) and far-red (Figs. 3D, 3F, 3H, 3J, and 3L) channels. Nonfluorescent dark pigments were still present but were no longer apically positioned within the RPE. Instead, they were now dispersed within the cytoplasm of the RPE in most of the AMD donors. In sum, our data detected an inverse relationship between the area of GA atrophy and the number of RPE cells and granules at the edge of the GA atrophy. However, donors with small size GA (Figs. 3C–3F) displayed the presence of bilaminar RPE and increased presence of both autofluorescent and nonautofluorescent granules.

Quantitation of autofluorescent granules beyond the edge of the GA lesion showed an age-related increase in the frequency of green/red fluorescence, and a decrease of nonfluorescent pigment granules. Far-red granules were first detected in a three-year-old donor. However, the amounts of these granules did not change significantly during aging and in AMD donors (Table 4). Additional representative images of the control tissue from donors with different ages are shown in Supplementary Figure S1. To further

Investigative Ophthalmology & Visual Science

Table 2. Human Donor Genotyping[*] and GA Atrophy Imaging Quantification

Donor ID	CFH Y402H	ARMS2 A69S	C3 R80G	HTRA Promoter	CFH I62V	SOD2	MBP	C80rf42	GA Area (mm^2)[†]
1	CC	GT	CC	AG	AG	AA	AC	AC	2.2 (OD), 2.7 (OS)
2	CT	GT	GG	AG	AG	AG	AA	CC	4.6 (OD), 6.2 (OS)
3	TT	GT	CG	AG	GG	AG	AC	AA	1.6 (OD), 1.6 (OS)
4	CC	GG	CG	GG	GG	AA	AA	CC	3.7 (OD)
5	CT	GG	CC	AG	GG	AG	AC	CC	1.7 (OD)
6	CC	GT	CG	AA	AG	AG	AA	AC	3.0 (OD); n.m. (OS)[‡]
7	CT	GT	CG	AG	AG	AG	AC	CC	3.8 (OD), 3.9 (OS)
8	CC	GG	CC	AG	GG	AG	AA	CC	0.9 (OD), 1.1 (OS)
9	CC	GG	CG	GG	GG	AG	AC	CC	2.3 (OD), 8.3 (OS)
10	TT	GG	CC	GG	GG	AG	AC	CC	1.6 (OD), 1.4 (OS)
11	CT	GT	CG	AG	GG	AG	AA	CC	1.7 (OD), 3.1 (OS)
12	CT	GG	GG	AG	GG	AG	CC	CC	6.6 (OD), 10.9 (OS)
13	CT	GT	CG	AG	GG	AG	AC	AC	0.5 (OD), 2.1 (OS)
14	CT	GT	CG	AG	GG	AA	AC	CC	2.1 (OD), 1.7 (OS)
15	CC	GT	CG	AG	GG	AA	AC	AA	1.0 (OD), 0.5 (OS)
16	CC	GG	CC	GG	GG	AG	CC	CC	1.6 (OD), 1.7 (OS)
17	CT	GT	CC	AG	AG	AA	AC	CC	1.7 (OD), 3.2 (OS)
C1	CT	GG	CC	GG	GG	AG	AC	AC	0
C2	CT	GG	CC	GG	AG	AG	AC	CC	0
C3	CT	GG	CG	GG	AG	AG	AC	CC	0
C4	CT	GT	CC	AG	GG	GG	AA	CC	0
C5	CT	GG	CC	GG	AG	AG	CC	AA	0
C6	CC	GT	GG	AG	AG	AA	AC	AC	0
C7	CC	GT	GG	AG	AG	GG	AA	AC	0
C8	CT	GG	CC	GG	AG	AG	AC	CC	0
C9	CC	GT	GG	GG	AG	GG	CC	CC	0
C10	CC	GG	GG	AG	AG	GG	CC	AC	0

Red font signifies risk alleles. CFH, complement factor H; ARMS2, age-related maculopathy susceptibility 2; HTRA1, high temperature requirement factor A1; C3, complement component 3; SOD2, superoxide dismutase 2; MBP, myelin basic protein; TDRP, testis development–related protein.

[*] Donor samples were genotyped for SNPs correlated with AMD and for SNPs previously shown to be associated with GA as previously reported.[18,19]

[†] Area: calculated from acquired IRAF-SLO images.

[‡] Not measured due to external damage to the globe in the area.

understand the nature of these granules, the same samples were processed and analyzed by transmission electron microscopy (Supplementary Fig. S2). At the ultrastructural level, melanin, lipofuscin, and melanolipofuscin granules were identified in all donors. This methodology did not identify a unique, different type of apical pigmented granule. The RPE from 38-week-old donor displayed melanosomes at different stages of maturation (M, Supplementary Fig. S1A). The RPE from a three-year-old donor displayed both melanosomes and a few lipofuscin granules (Lip, Supplementary Fig. S1B). The cytoplasm of the RPE from a 72-year-old donor is filled with lipofuscin granules (Supple-

Investigative Ophthalmology & Visual Science

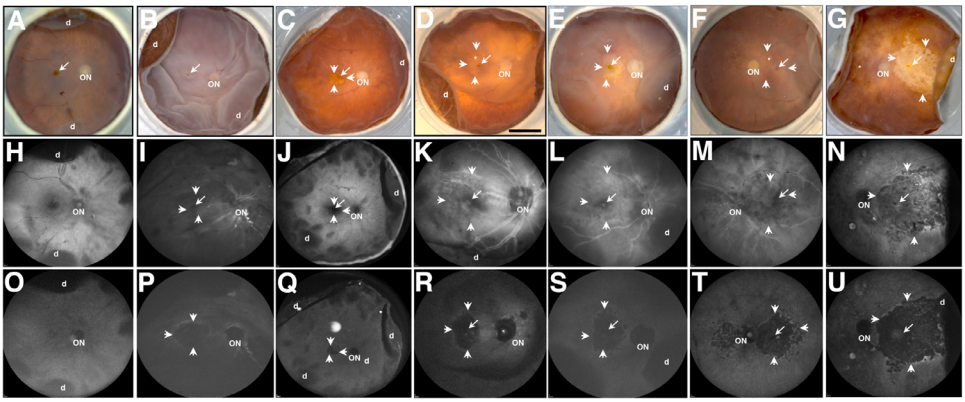

Figure 1. Ex vivo imaging of representative AMD donor eyes with GA. Fundus images (**A–G**), BAF-SLO (**H–N**), and IRAF-SLO (**O–U**) images were acquired. Representative images of control (**A**), AMD donors with small (**E, G**), medium (**C, D**), and large (**B, F**) GA area were obtained; GA is visible in all three imaging modalities. Visualization in BAF-SLO and IRAF-SLO identified areas of fovea (*arrow*), optic nerve (*ON*), and hyper-autofluorescence in GA edges (*small arrows*). D, retinal detachment. Scale bar: 0.5 cm.

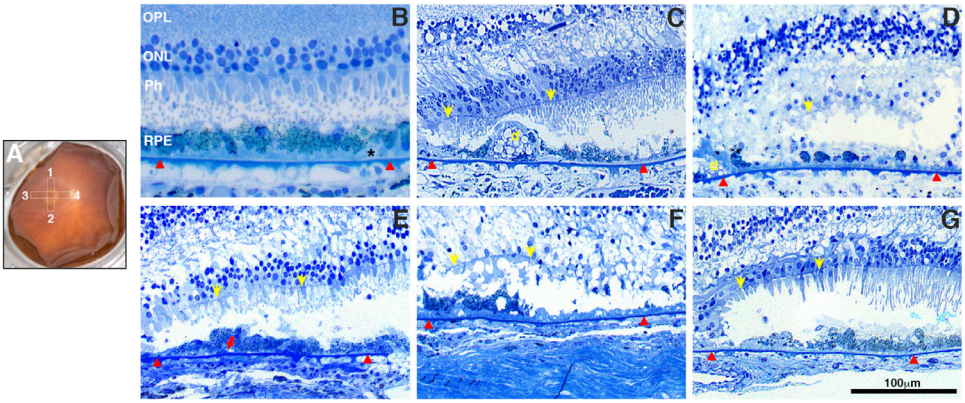

Figure 2. Histologic morphology of RPE and retina in GA borders of donors with AMD. Fundus image of a control eye (**A**, *OD*) with a schematic drawing of the GA areas harvested and processed for further analysis. These include the superior (region 1), nasal (region 4), temporal (region 3), and inferior (region 2). Toluidine blue–stained plastic sections (1 μm) of retinas from all AMD donors and an age-similar control. Morphologic study of the control retina (**B**) displayed typical retinal lamina, slightly "nonuniform" RPE structure, and pigmentation with small patches of early basal laminar deposit (BLamD, *) over the Bruch's membrane (*red arrowheads*). Histologic study in the edge of the GA atrophy of AMD donors displayed degenerated photoreceptors and RPE. Observed RPE degeneration morphology included "very nonuniform" RPE (**C**), "dissociated" RPE (**D**), "shedding" RPE (**E**); "bilaminar" RPE (**F**), and "sloughed" RPE (**G**). *Yellow arrows* show ELM (external limiting membrane) descending toward the Bruch's membrane to define the GA border; *red arrows* show shed RPE contents. D, drusen. Scale bar: 100 μm.

mentary Fig. S1C). In comparison, the cytoplasm of an 85-year-old AMD donor (no. 16), outside the GA also display a large number of lipofuscin and just a few melanin granules (Supplementary Fig. S1D).

Immunocytochemistry at the Border of GA

Pathology of AMD lesions typically demonstrates signs of persistent chronic inflammatory damage, including not

Table 3. Summary of Frequency of RPE Morphology Within the GA Border

RPE Morphology*	Description*	Frequency of Distribution (%)†
Very Nonuniform	Slightly nonuniform morphology and pigmentation	48.84
Sloughed	Intact epithelium with spherical cells sloughed into subretinal space	32.56
Shedding	Intact epithelium with basal shedding of nonnucleated granule aggregates into BLamD	19.77
Bilaminar	Double layers	9.30
Intraretinal	Intraretinal	3.49
Dissociated	Nucleated non-contacting, individual RPE	37.21

* Terms and descriptions defined in Zanzottera et al. 2015 [24].
† Frequency calculated from all the quantified RPE phenotype in both epon-embedded and cryosections within 200 μm of the GA border. A total of 86 different regions in all 32 eyes from AMD donors were analyzed.

Investigative Ophthalmology & Visual Science

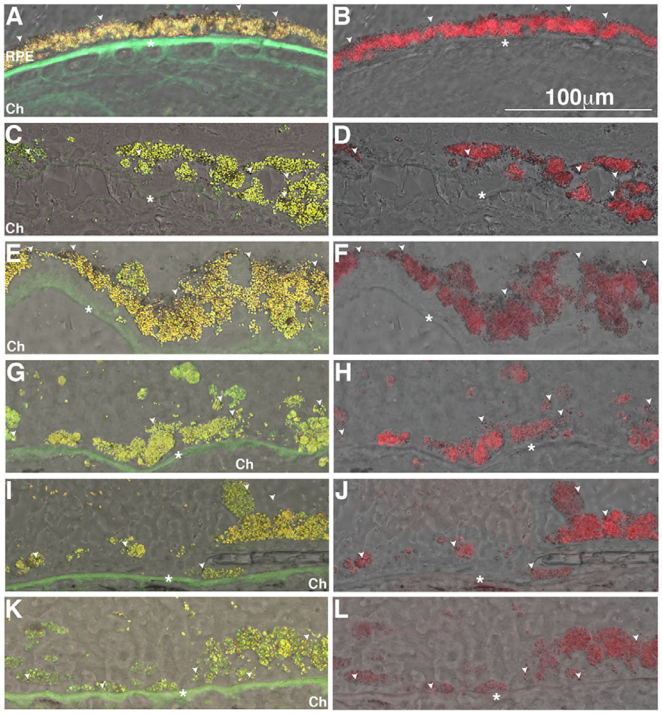

Figure 3. Accumulation of autofluorescent granules in the RPE in GA borders of donors with AMD. Representative bright field images overlaid with epifluorescence image in the green-red (**A, C, E, G, I, K**) and far-red (**B, D, F, H, J, L**) channels. Human cryosections of a matched control (**A, B**) and AMD donor eyes at the GA border (**C–L**) were observed on epifluorescence in the green-red and far-red channels; autofluorescence was merged into bright field images. The RPE from a control eye showed the prevalence of granules fluorescent in the green-red (**A**) and far-red (**B**) channels and a several dark-pigment non-fluorescent granules aligned along the apical surface (*white arrowheads*). The AMD donor eyes at the GA border (**C–L**) displayed hypertrophic RPE cells with their cytoplasm filled with granules fluorescent both in the green-red and far-red channels; a few dark-pigment nonfluorescent granules are present and distributed through the cytoplasm. Ch, choroid. Scale bar: 100 µm. * Bruch's membrane.

Table 4. Summary of Frequency of RPE Granules Beyond the Edge of the GA Lesion or Within Control Retinas

Donor information	Frequency of Green/Red Fluorescent Granules (%)	Frequency of Far Red Fluorescent Granules (%)	Frequency of Pigmented and Non-Fluorescent Granules (%)
Control donor (38 week-old)	0	0	100
Control donor (3 years old)	15.25	44.48	34.16
Control donor (7 years old)	32.29	42.91	24.80
Control (non-AMD, 66–91 years old)	49.61	33.78	16.60
AMD Donors, Outside GA	44.95	42.31	12.75
AMD Donors, small size GA	50.82	42.01	7.17
AMD Donors, medium size GA	48.36	39.33	10.98
AMD Donors, large size GA	48.57	38.77	12.66

Frequency calculated from cryosections within 200 µm of the GA border. A total of 87 different regions in all eyes were analyzed.

only infiltration of macrophages and accumulation of microglia, but also the presence of inflammatory components such as complement factors, and pro-inflammatory cytokines/chemokines as previously described.[4,25] Thus we immunostained these tissues for markers of components of the complement system (CFH and C5b-9, Fig. 4) and immune cells (Iba1, and CD68, Fig. 5) within 400 µm of the GA atrophy margin.

Complement factor H is one of two predominant cell surface-associated alternative pathway inhibitors localized in the RPE-choroid complex.[26] In control retinas (Fig. 4A, arrowheads), CFH displayed major distribution throughout the choroidal stroma with focal regions of more intense immunoreactivity associated with choroidal vasculature and the matrix, as previously described.[27] Minor distribution of CFH was also observed in the neurons in the GCL, in the plexiform layers and photoreceptor inner segments as previously reported.[28] Increased CFH immunoreactivity was observed in the retina of donors with small and large size GA atrophy (Figs. 4B, 4D) but was decreased in donors with medium-size GA atrophy (Fig. 4C).

The terminal complement complex C5b-9 is the neoepitope that forms after assembly of the MAC. In control retinas (Fig. 4E, arrowheads), C5b-9 displayed weak diffuse pattern in the BM/basal surface of the RPE, with occasional spotty presence in cytoplasm of "damaged" or hypertrophic cells as previously reported.[29] Increased C5b-9 staining was observed in the retina of donors with GA atrophy (Figs. 4F, 4G, and 4H). Increased distribution of C5b-9 was also observed in the RGC layer, and in plexiform layers of

Investigative Ophthalmology & Visual Science

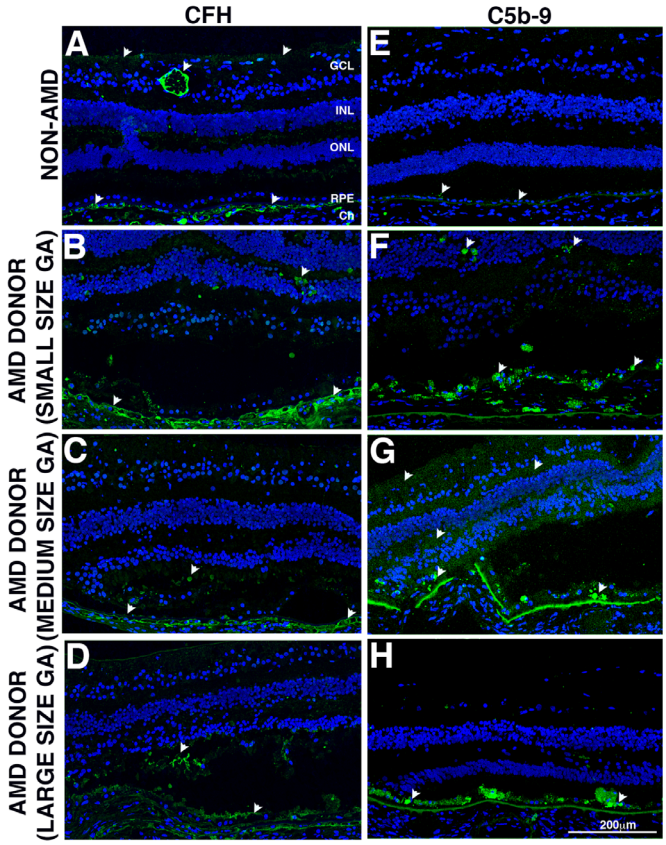

Figure 4. Immunocytochemistry of retinal sections in the GA borders of donors with AMD stained with complement antibodies. Immunofluorescence of control and AMD retinal sections labeled with antibodies to CFH (**A, B, C, D**) and C5b-9 (**E, F, G, H**). The control retina displayed CFH deposition in the choroid vessels, ganglion cell layer, and retinal vessel (*white arrowheads*). Minor reaction was also present in the plexiform layers and photoreceptor inner segments. The AMD donors with small- and large-size GA atrophy (**B, D**) displayed increased CFH deposition in the choroid vessels. On the other hand, CFH was decreased in AMD donors with medium size GA atrophy (**C**). The AMD donors also displayed increased CFH deposition in the plexiform layers and photoreceptor inner segments. In the control retinas immunohistologic staining with C5b-9 display weak diffuse pattern in the Bruch's membrane (BM)/basal surface of the RPE (**E**). Increased C5b-9 staining was observed in the retina of donors with GA atrophy (**F–H**). Increased distribution of C5b-9 was also observed in the RGC layer, and in plexiform layers of the donors with small and medium size GA atrophy (**F, G**) but not in donors with large size GA atrophy (**H**), where the majority of C5b-9 distributed in the RPE Bruch's membrane (BM)/basal surface and cytoplasm. For all images, the atrophy was located at the left edge of the picture; image breaks in BM (**G**) is an artifact from processing. Scale bar: 200 µm.

the donors with small and medium-size GA atrophy (Figs. 4F, 4G, arrowheads). C5b-9 was not elevated in donors with large size GA atrophy (Fig. 4H), where the majority of C5b-9 distributed in the RPE cytoplasm and BM.

Quantification of CFH labeling showed a significant increase in the deposition in large size GA lesions compared with medium-size GA lesions within 200 µm and 400 µm of the GA border (Supplementary Fig. S3). A trend of increase in the CFH deposition in sections from AMD donors outside the GA lesions and in the samples with small size GA lesions was observed within 400 µm of the GA border. A significant increase in the C5b-9 deposition was identified in the small size GA lesions compared with control samples within 400 µm of the GA border (Supplementary Fig. S3).

The retina of donors with GA lesions (Figs. 5B–5D) identified numerous mislocalized Iba-1 + cells by immunohistochemistry, presumed to be microglia that were noticeably absent in control donor sections (Fig. 5A). In the control retinas, Iba-1+ cells were observed extending processes mostly within the NFL-GCL, IPL, INL, OPL, OS, and choroid. However, in the retina of donors with GA lesions more Iba-1+ cells were observed, and their processes were also observed penetrating the layer perpendicularly; a significant number of Iba-1+ cells were observed in the photoreceptor outer segments. Donors with small and medium-size GA lesions (Figs. 5B, 5C) displayed the increased presence of Iba-1+ cells in all layers of retina and infiltration in the outer segments of the photoreceptor cells. Donors with large size GA lesions exhibited increased Iba-1+ cells versus control samples, but these cells are more ameboid and migrating towards photoreceptor outer segments and RPE/BM (Fig. 5D). Additional labeling of the tissue with markers of both rods (rhodopsin) and cones (red/green opsin) and Iba-1 showed that the Iba-1 + cells were mostly associated with the cone outer segments in the control. However, in GA samples Iba-1+ cells distribution was evident in both inner and outer segments (Supplementary Fig. S3).

Quantification of Iba-1 + cells evidenced an increase in AMD tissue with GA lesions when compared to control donor sections (Supplementary Fig. S4). An increasing trend in the presence of Iba-1+ cells was detected in sections from AMD donors with GA lesions and specifically in the samples with small and medium-size GA lesions. A significant increase in Iba-1+ cells was identified in medium-size GA lesions compared to AMD samples outside GA lesions and control samples within 200 µm of the GA border. A

Investigative Ophthalmology & Visual Science

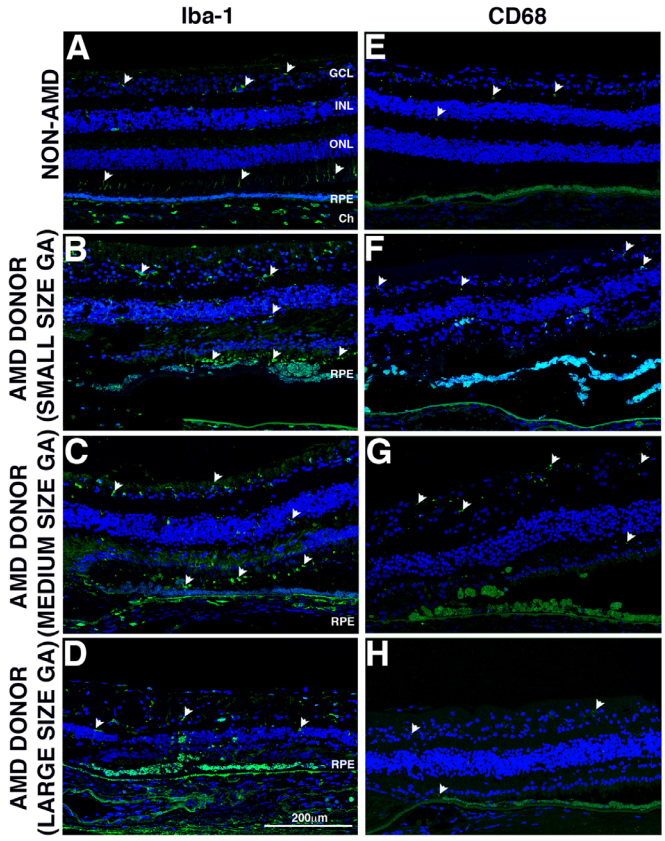

Figure 5. Immunocytochemistry of retinal sections in the GA borders of donors with AMD stained with inflammatory cell marker antibodies. Immunofluorescence of control and AMD retinal sections labeled with antibodies to Iba-1 (**A, B, C, D**) and CD68 (**E, F, G, H**). Non-AMD donor displayed very few Iba-1+ cells in their retinas, with cells mostly localized in the inner retina, but there were a few also localized to the photoreceptor outer segments (**A**, *white arrowheads*). The AMD donors with small and medium size GA atrophy (**B, C**) displayed infiltration of Iba-1+ cells in the outer retina; these cells displayed an amoeboid phenotype. However, fewer Iba-1+ cells were present in the retinas of AMD donors with big size GA atrophy (**D**). Non-AMD donor (**E**) displayed very few CD68+ cells in their retinas. The AMD donors with small and medium size GA atrophy displayed increased presence of CD68+ cells in the inner retina (**F, G,** *white arrowheads*). However, CD68+ cells were mostly absent from AMD donors with big size GA atrophy (**D**). For all images, the atrophy was located at the left edge of the picture. Scale bar: 200 μm.

significant decrease in Iba-1+ cells was observed in the large size GA lesions in both the 0–200 and 200–400 μm of the GA border when compared with the medium-size GA lesions.

Macrophages were identified by labeling with CD68 antibodies (Figs. 5E–5H). CD68 immunostaining of macrophages was rarely observed in the soma of few round cells in the NFL-GCL and plexiform layers of control non-AMD donors (Fig. 5E, arrowheads). The increased presence of patches of CD68 staining was observed in the retina of donors with GA lesions (Fig. 5F–5H); their distribution was mostly associated with the NFL-GCL and outer segments. Donors with small- and medium-size GA atrophy (Figs. 5F. 5G) showed elevated CD68 staining when compared with donors with large-size GA atrophy (Fig. 5H).

These data suggest that inflammatory cells such as microglia, macrophages, or other cells expressing these markers are associated with and have a prominent role in GA atrophy.

Discussion

To date, there are no approved treatments to prevent the onset and progression of GA. Treatment strategies aimed at improving long-term visual acuity outcomes to stop or slow the nonexudative AMD at an earlier stage are needed. However, vision loss takes many years to develop in this type of AMD. Recently, the international group of experts of the Classification of Atrophy Meeting group analyzed and discussed the anatomic biomarkers that predict GA development using OCT.[30,31] Among the several issues discussed were to explore new strategies to identify and determine AMD early stages endpoints. Thus understanding the composition of the cells in and around the areas of cellular loss in GA pathology is critical to generate new data that will help both to understand better the current clinical trial endpoint and also to show why earlier endpoints are needed. Earlier research showed dramatic changes in RPE morphology within 500 μm of the atrophy border.[11,32,33] Thus we concentrated our observations to within 400 μm of the leading edge of the GA and compared our findings to observations in control and AMD tissue outside of the GA (perimacular area).

Melanin, lipofuscin, and melanolipofuscin compose the three populations of pigment granules present in human RPE. Melanin granules develop early in embryogenesis; they are present in all RPE cells of embryos after seven weeks of age.[34] Melanosomes undergo a well-documented four-stage maturation previously described.[34,35] By 27 weeks of

Investigative Ophthalmology & Visual Science

gestation, all melanosomes are melanized and are stage IV granules.[36] In our 38-week-old donor eye, the melanin granules were easily identifiable. Melanin acts as a cellular antioxidant and is supposed to protect RPE cells by scavenging free radicals, quenching electronically excited states, and sequestering redox-active metal ions elicited by visible light or by redox-active metal ions.[37–40] Indeed, the oxidation of melanin and its irreversible bleaching has been induced by aerobic irradiation of melanin with ultraviolet or visible light.[41–43] Electron paramagnetic resonance spectroscopy observation of RPE cells from human donors first detected an age-related loss content of melanin in RPE cells.[42] Additional data suggested that this age-dependent decrease of melanin granules is due to the remodeling of pigment granules by lytic enzymes and promoting complex melanin granules in the form of melanolipofuscin.[34,44]

Lipofuscin is a fluorescent heterogeneous lipid- and bisretinoids-rich aggregate accumulated with age and in AMD in the RPE cytoplasm.[1–3] In these cells, lipofuscin is derived primarily from phagocytosis of shed photoreceptor outer segment membranes,[34] and from RPE autophagocytosis material.[45]

The optical characteristics of melanin and lipofuscin granules purified from whole eyes have been previously reported.[46] Melanin granules isolated from fetal eyes between 12 and 22 weeks of gestation displayed weak fluorescence intensity with an excitation peak at 350 nm and an emission peak around 450 nm. However, a secondary peak at ~570 nm, extending from 500 to 700 nm, was observed starting from the 5- to 29-year-old age group. Lipofuscin granules exhibited a broad emission spectrum with a peak at 600 nm when excited at ~364 nm.[46] This emission peak remained unchanged because the excitation wavelength was set at 476 nm. Additional analysis of the emission spectra from the various age groups showed four main spectral regions of interest in isolated lipofuscin granules: a blue-green shoulder located at 470 nm, a green-yellow shoulder at 550 nm, the main peak located at 600-610 nm, and a far-red shoulder at 680 nm. The blue-green and green-yellow peaks were evident in the 5- to 29-year-old and the 30- to 49-year-old age group, but it was not present in the >50-year-old age group. In contrast, the far-red fluorescence peak was shown to increase with age consistently.

The previous report by Keilhauer and Delori[12] supported a role for melanin in near-infrared AF arising primarily from the RPE cells with some contribution from the melanin in the choroid. The authors' conclusions were supported by (1) high foveal AF, which corresponded with the distribution of RPE melanin; (2) AF in clumps of stacked or hyperpigmented RPE cells in the subretinal and sub-RPE space; (3) reduced AF in geographic and peripapillary atrophy; and (4) AF from pigmented epithelium cells of the iris. Although the role for melanin in near-infrared AF was clearly delineated in this study, the resolution to separate it from (photo)oxidized melanin was insufficient. Furthermore, the authors pondered that they could not rule out that the excitation spectrum of one of the lipofuscin fluorophores extends to and contributes to the near-infrared AF.

Additional reports imaging Stargardt disease 1 (STGD1) patients carrying mutations in the *ABCA4* gene and Abca4$^{-/-}$ mice challenged the assumption that near-infrared AF originates only from melanin.[47,48] STGD1 patients, with central RPE atrophy, displayed gray level near-infrared AF intensity values consistently elevated. Similarly, Abca4$^{-/-}$ agouti mice, a model of accelerated formation of bisretinoid lipofuscin, also displayed increased near-infrared AF signal.[49] Finally, a very recent manuscript analyzing the near-infrared AF properties of melanin in mice cryosections concluded that melanin is not fluorescent in this wavelength.[50]

In this study no far-red fluorescence signal was detected from the melanin granules in a 38-week-old donor but was detected in a three-year-old donor. Interestingly, the far-red signal in our samples increased in intensity during aging. Thus our present data and the previous reports cited above suggest that melanin near-infrared AF is a consequence of photic and oxidative stress and that lipofuscin also fluoresce in this wavelength when in high concentrations.

Throughout aging, a layer of pigmented non-fluorescent granules was observed at the apical surface of the RPE in both control and AMD donors. Melanin and lipofuscin typically localize to different positions within the cell: melanin is apical, and lipofuscin is central to basal.[34,35] Because of their morphology and cellular distribution, we hypothesized that the apical nonfluorescent granules represent nonfluorescent melanin granules. Additional experiments are needed to identify the chemical composition of these granules. Our hypothesis is that these apical pigment granules might quench the fluorescent signal generated from melanin and lipofuscin granules metabolically modified within the RPE cells. Thus the increased autofluorescence surrounding the GA lesion border would result from the loss and dislocation of the melanin granules typically present in the RPE apical region, as shown in Figure 6.

A recent meta-analysis of 11 studies reported that GA progression rate in the outer zone of the macula (1800–3000 µm from the foveal center) was 3.2-fold faster than the growth rate in the inner zone of the macula (0–500 µm from the foveal center).[51] The study also suggested that the occurrence of different shapes of GA lesions might be related to the fact that the GA growth rate changes at different retinal locations, leading GA lesions to evolve into the various shapes at different time point. In the present study, we analyzed the GA lesion border in four different regions but found no common features within these in the different donors.

At the histological level, studies of the RPE and retina in the GA and surrounding areas have reported a steady progression of worsening RPE morphology towards the atrophic area.[11,32] Recently, a histology-based taxonomy of morphologic phenotypes used to define the RPE stress-response repertoire in AMD was introduced to study the GA transition.[24,52] In this study, we identified these same RPE phenotypes in our GA samples. We showed that most of the RPE cells at the GA lesions margins displayed very nonuniform, dissociated, and sloughed RPE morphology. RPE cells of the sloughed phenotype alter their cellular profile to express smooth muscle actin (α-SMA), upregulate the intermediate filament vimentin, and repress cytokeratin.[53] In AMD, some degenerated RPE cells appear to undergo epithelial-to-mesenchymal transition (EMT) due to loss of normal cell shape, loss of their junctional integrity exhibiting migratory behavior, and expression of mesenchymal markers such as α-SMA.[53–57] Our study detected hypertrophic RPE cells, without the typical epithelial phenotype, with their cytoplasm filled with granules fluorescent both in the far-red and green-red channels in the leading edges of GA lesions. Thus our data support the hypothesis that the RPE cells on the leading edge of GA lesions are undergoing transdifferentiation, including potentially, EMT.

Investigative Ophthalmology & Visual Science

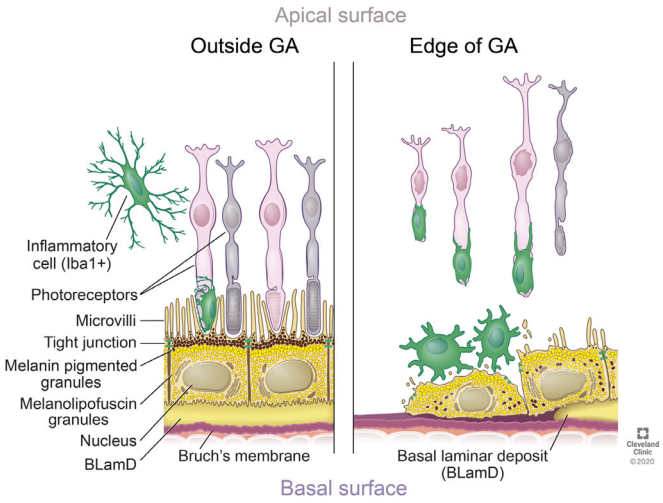

Figure 6. Schematic model of the main features identified of the RPE in and out of the GA borders. The RPE outside the GA area display apical melanin granules. Their cytoplasm is filled with lipofuscin, melanolipofuscin, or both. The RPE at the edge of the GA is hypertrophic, displays decreased melanin pigmented granules and these are disorderly distributed in the cytoplasm. There is an increase in the presence of microglia in the retina in the edge of the GA when compared with retinas of control and AMD donors outside the GA. The microglia in the edge of the GA display activated morphology. Reprinted with permission, Cleveland Clinic Center for Medical Art & Photography © 2020. All Rights Reserved.

Drusen accumulate between the RPE basal lamina and the inner collagenous layer of BM. Drusen formation increases an individual's risk of developing advanced AMD and is visible by fundus color photography, autofluorescence, and spectral domain optical coherence tomography (SD-OCT).[58,59] Identification of complement factor proteins in drusen isolated from whole eyecups from donors with AMD,[60] coupled with genetic variation in several complement factor genes in AMD patients[61–64] implicates inflammation in the pathogenesis of AMD. Here, we investigated CFH, the major fluid phase inhibitor of the alternative complement pathway, and C5b-9, the cytolytic membrane attack complex that leads to the cell death via cell lysis in the leading edges of GA lesion.

The CFH protein is present in the RPE, photoreceptor inner segments, in the inner and outer plexiform layers, and the ganglion cell layer in the retina.[28] The CFH labeling was mostly present in the choroid of the retinas from control donors whereas in AMD donors with GA lesions, the primary distribution of CFH was in drusen, the RPE, choroid, and remaining photoreceptor inner segments. Expression of CFH in RPE cells is induced by the proinflammatory cytokine interferon-gamma[65] and by induction of oxidative stress.[66] Thus the inflammation present in the macular region could account for the observed increase in CFH labeling in the retinas from AMD donors with GA lesions. Our study is consistent with a previous one that reported high CFH immunoreactivity in the choroid and drusen of AMD donors but no differences in CFH-labeling patterns between genotypes of individuals carrying the high-risk 402HH polymorphism genotype.[27] A study in a large number of AMD donor eyes reported that in early AMD, MAC was exclusively associated with the choriocapillaris, while in advanced AMD it was observed in both the choriocapillaris and RPE.[67] Our data suggest that in a normal eye, MAC deposition is primarily on the endothelia of the choroidal capillaries with minor deposition on the inner retinal blood vessels. However, in GA tissue, MAC deposition differentially increased with the lesion size. We hypothesize that in a pathologic situation such as AMD the MAC would also start to deposit on the RPE membrane and would keep building up over time while RPE keeps secreting CFH. At the same time, RPE phagocytose and internalize any deposits on the membrane as a mean to defend itself from the damaging lytic effect of MAC.

Within the retina, there are two sources of inflammatory cells. Microglia are resident macrophages derived from yolk sac progenitors during embryogenesis. Monocyte-derived macrophages can infiltrate the tissue during disease and are derived from the bone marrow. Conflicting evidence from animal models suggests that resident and invading macrophages/microglia can both prevent and promote neovascular AMD. In GA AMD, this issue still remains unclear.[15] Recent data from tissue from donors with AMD and animal models suggested that complement activation on photoreceptors contributed to the loss of photoreceptor function in C5a-dependent recruitment of peripheral blood monocytes independent of resident microglia.[68] A previous report failed to detect a significant number of inflammatory cells in the early stages of AMD.[69] However, the density of Iba1+ cells was significantly increased in the retina and choroid of sections from three AMD donor[70] and in tissue from a donor with advanced-stage AMD.[71] Also, significantly more activated macrophages were identified and quantified in GA eyes, within the area of submacular choroid associated with RPE atrophy compared with control eyes in GA eyes.[72] Here, we observed an increased presence of Iba-1+ cells in the leading edge of the small and medium size GA lesions. Iba-1 + cells were mostly associated with the cone outer segments in the control samples but were associated with both inner and outer segments in the GA. We also found that although an increased number of CD68 positive cells were present in the leading edge of the GA lesions, the overall number of these cells was small.

Altogether, we detected the most significant changes in inflammation markers in AMD donors with medium-size GA lesions including, the increased presence of Iba-1+ cells distributed in the retina, RPE and choroid, increased deposition of CFH in the choroid vessels, and presence of CD68+ cells in their retinas. Also, C5b-9 immunostaining was amplified in these GA AMD eyes versus control subjects, but the

Investigative Ophthalmology & Visual Science

changes were not significant among the groups of different GA size. This apparent increase in inflammatory reactivity represents only a snapshot in time making it impossible to infer whether the increased presence of activated microglia and macrophage in the edge of the GA lesions prevents or promotes atrophy. Future investigations of AMD eye donors at different stages of the disease are required to further investigate the immune-mediated pathologic mechanism.

Our study represents the first attempt to investigate cellular-level fluorescence imaging and detailed analysis of the RPE AF granules using filters similar in excitation and emission wavelength ranges as those used by BAF- and IRAF-SLO imaging modalities in the ophthalmology clinics of GA pathology. A strength of this study is the number of human eyes from donor eyes with GA. This study resulted in tangible improvements of our understanding of AMD pathology with two potential limitations. First, it provides information from a single time point in the GA AMD course of donors that lacked in comprehensive historical clinical information. Another limitation is the influence of the orientation of the tissue analyzed (e.g., en face versus radial sections) on the collection of data and interpretation of the results because undoubtedly, different optical properties are encountered between these two methods. In closing, presented data further aid in our understanding and interpretation of BAF- and IRAF-SLO clinical imaging phenotypes from AMD patients with GA.

Acknowledgments

The authors thank David Schumick for preparation of the illustration on the RPE in and out of the GA border and Shannan Eddington for her EM technical support.

Supported by the National Institutes of Health (EY027750 to VLB and EY025002 to RAR), National Eye Institute P30 Core Grants (P30EY025585 to the Cleveland Clinic and P30EY000331 to UCLA), The Wolf Family Foundation, a Research to Prevent Blindness Challenge Grant, The BrightFocus Foundation (M2016079 to VLB), a Cleveland Eye Bank Foundation Institute Grant, and Cleveland Clinic Foundation startup funds. The authors also acknowledge the support of Foundation Fighting Blindness in setting up the Eye Tissue Repository and the Cleveland Clinic for funding its maintenance.

Disclosure: **V.L. Bonilha,** None; **B.A. Bell,** None; **J. Hu,** None; **C. Milliner,** None; **G.J. Pauer,** None; **S.A. Hagstrom,** None; **R.A. Radu,** None; **J.G. Hollyfield,** None

References

1. Ng KP, Gugiu B, Renganathan K, et al. Retinal pigment epithelium lipofuscin proteomics. *Mol Cell Proteomics*. 2008;7:1397–1405.
2. Sparrow JR, Wu Y, Kim CY, Zhou J. Phospholipid meets all-trans-retinal: the making of RPE bisretinoids. *J Lipid Res*. 2010;51:247–261.
3. Sparrow JR, Gregory-Roberts E, Yamamoto K, et al. The bisretinoids of retinal pigment epithelium. *Prog Retin Eye Res*. 2012;31:121–135.
4. Ding X, Patel M, Chan CC. Molecular pathology of age-related macular degeneration. *Prog Retin Eye Res*. 2009;28:1–18.
5. Ach T, Tolstik E, Messinger JD, Zarubina AV, Heintzmann R, Curcio CA. Lipofuscin redistribution and loss accompanied by cytoskeletal stress in retinal pigment epithelium of eyes with age-related macular degeneration. *Invest Ophthalmol Vis Sci*. 2015;56:3242–3252.
6. Brandstetter C, Mohr LK, Latz E, Holz FG, Krohne TU. Light induces NLRP3 inflammasome activation in retinal pigment epithelial cells via lipofuscin-mediated photooxidative damage. *J Mol Med*. 2015;93:905–916.
7. Delori FC, Dorey CK, Staurenghi G, Arend O, Goger DG, Weiter JJ. In vivo fluorescence of the ocular fundus exhibits retinal pigment epithelium lipofuscin characteristics. *Invest Ophthalmol Vis Sci*. 1995;36:718–729.
8. Sunness JS, Margalit E, Srikumaran D, et al. The long-term natural history of geographic atrophy from age-related macular degeneration: enlargement of atrophy and implications for interventional clinical trials. *Ophthalmology*. 2007;114:271–277.
9. Holz FG, Bellman C, Staudt S, Schutt F, Volcker HE. Fundus autofluorescence and development of geographic atrophy in age-related macular degeneration. *Invest Ophthalmol Vis Sci*. 2001;42:1051–1056.
10. Pfau M, Goerdt L, Schmitz-Valckenberg S, et al. Green-light autofluorescence versus combined blue-light autofluorescence and near-infrared reflectance imaging in geographic atrophy secondary to age-related macular degeneration. *Invest Ophthalmol Vis Sci*. 2017;58:BIO121–BIO130.
11. Zanzottera EC, Ach T, Huisingh C, Messinger JD, Spaide RF, Curcio CA. Visualizing retinal pigment epithelium phenotypes in the transition to geographic atrophy in age-related macular degeneration. *Retina*. 2016;36(Suppl 1):S12–S25.
12. Keilhauer CN, Delori FC. Near-infrared autofluorescence imaging of the fundus: visualization of ocular melanin. *Invest Ophthalmol Vis Sci*. 2006;47:3556–3564.
13. Grieve K, Gofas-Salas E, Ferguson RD, Sahel JA, Paques M, Rossi EA. In vivo near-infrared autofluorescence imaging of retinal pigment epithelial cells with 757 nm excitation. *Biomed Opt Express*. 2018;9:5946–5961.
14. Hageman GS, Luthert PJ, Victor Chong NH, Johnson LV, Anderson DH, Mullins RF. An integrated hypothesis that considers drusen as biomarkers of immune-mediated processes at the RPE-Bruch's membrane interface in aging and age-related macular degeneration. *Prog Retin Eye Res*. 2001;20:705–732.
15. Ambati J, Atkinson JP, Gelfand BD. Immunology of age-related macular degeneration. *Nature Rev Immunol*. 2013;13(6):438–451.
16. Curcio CA. Soft drusen in age-related macular degeneration: biology and targeting via the oil spill strategies. *Invest Ophthalmol Vis Sci*. 2018;59:AMD160–AMD181.
17. Cherepanoff S, McMenamin P, Gillies MC, Kettle E, Sarks SH. Bruch's membrane and choroidal macrophages in early and advanced age-related macular degeneration. *Br J Ophthalmol*. 2010;94:918–925.
18. Hagstrom SA, Ying GS, Pauer GJ, et al. Pharmacogenetics for genes associated with age-related macular degeneration in the Comparison of AMD Treatments Trials (CATT). *Ophthalmology*. 2013;120:593–599.
19. Sobrin L, Ripke S, Yu Y, et al. Heritability and genome-wide association study to assess genetic differences between advanced age-related macular degeneration subtypes. *Ophthalmology*. 2012;119:1874–1885.
20. Bonilha VL, Rayborn ME, Bell BA, Marino MJ, Fishman GA, Hollyfield JG. Retinal histopathology in eyes from a patient with stargardt disease caused by compound heterozygous ABCA4 mutations. *Ophthalmic Genet*. 2015:1–11.
21. Sunness JS, Gonzalez-Baron J, Applegate CA, et al. Enlargement of atrophy and visual acuity loss in the geographic atrophy form of age-related macular degeneration. *Ophthalmology*. 1999;106:1768–1779.

Investigative Ophthalmology & Visual Science

22. Fleckenstein M, Mitchell P, Freund KB, et al. The progression of geographic atrophy secondary to age-related macular degeneration. *Ophthalmology*. 2018;125:369–390.
23. Fleckenstein M, Charbel Issa P, Helb HM, et al. High-resolution spectral domain-OCT imaging in geographic atrophy associated with age-related macular degeneration. *Invest Ophthalmol Vis Sci*. 2008;49:4137–4144.
24. Zanzottera EC, Messinger JD, Ach T, Smith RT, Freund KB, Curcio CA. The Project MACULA retinal pigment epithelium grading system for histology and optical coherence tomography in age-related macular degeneration. *Invest Ophthalmol Vis Sci*. 2015;56(5):3253–3268.
25. Sennlaub F, Auvynet C, Calippe B, et al. CCR2(+) monocytes infiltrate atrophic lesions in age-related macular disease and mediate photoreceptor degeneration in experimental subretinal inflammation in Cx3cr1 deficient mice. *EMBO Mol Med*. 2013;5:1775–1793.
26. Anderson DH, Radeke MJ, Gallo NB, et al. The pivotal role of the complement system in aging and age-related macular degeneration: hypothesis re-visited. *Prog Retin Eye Res*. 2010;29:95–112.
27. Johnson PT, Betts KE, Radeke MJ, Hageman GS, Anderson DH, Johnson LV. Individuals homozygous for the age-related macular degeneration risk-conferring variant of complement factor H have elevated levels of CRP in the choroid. *Proc Natl Acad Sci USA*. 2006;103:17456–17461.
28. Mandal MN, Ayyagari R. Complement factor H: spatial and temporal expression and localization in the eye. *Invest Ophthalmol Vis Sci*. 2006;47:4091–4097.
29. Anderson DH, Mullins RF, Hageman GS, Johnson LV. A role for local inflammation in the formation of drusen in the aging eye. *Am J Ophthalmol*. 2002;134:411–431.
30. Holz FG, Sadda SR, Staurenghi G, et al. Imaging protocols in clinical studies in advanced age-related macular degeneration: recommendations from classification of atrophy consensus meetings. *Ophthalmology*. 2017;124:464–478.
31. Sadda SR, Guymer R, Holz FG, et al. Consensus definition for atrophy associated with age-related macular degeneration on OCT: classification of atrophy report 3. *Ophthalmology*. 2018;125:537–548.
32. Sarks JP, Sarks SH, Killingsworth MC. Evolution of geographic atrophy of the retinal pigment epithelium. *Eye*. 1988;2:552–577.
33. Rudolf M, Vogt SD, Curcio CA, et al. Histologic basis of variations in retinal pigment epithelium autofluorescence in eyes with geographic atrophy. *Ophthalmology*. 2013;120:821–828.
34. Feeney-Burns L. The pigments of the retinal pigment epithelium. In: *Current topics in eye research*. Vol. 2. Academic Press, Inc.; 1980:119–178.
35. Boulton ME. Studying melanin and lipofuscin in RPE cell culture models. *Exp Eye Res*. 2014;126:61–67.
36. Stroeva OG, Mitashov VI. Retinal pigment epithelium: proliferation and differentiation during development and regeneration. *Int Rev Cytol*. 1983;83:221–293.
37. Ostrovsky MA, Sakina NL, Dontsov AE. An antioxidative role of ocular screening pigments. *Vision Res*. 1987;27:893–899.
38. Sarna T. Properties and function of the ocular melanin—a photobiophysical view. *J Photochem Photobiol B*. 1992;12:215–258.
39. Rozanowski B, Burke JM, Boulton ME, Sarna T, Rozanowska M. Human RPE melanosomes protect from photosensitized and iron-mediated oxidation but become pro-oxidant in the presence of iron upon photodegradation. *Invest Ophthalmol Vis Sci*. 2008;49:2838–2847.
40. Hong L, Simon JD. Current understanding of the binding sites, capacity, affinity, and biological significance of metals in melanin. *J Phys Chem B*. 2007;111:7938–7947.
41. Korytowski W, Sarna T. Bleaching of melanin pigments. Role of copper ions and hydrogen peroxide in autooxidation and photooxidation of synthetic dopa-melanin. *J Biol Chem*. 1990;265:12410–12416.
42. Sarna T, Burke JM, Korytowski W, et al. Loss of melanin from human RPE with aging: possible role of melanin photooxidation. *Exp Eye Res*. 2003;76:89–98.
43. Biesemeier A, Kokkinou D, Julien S, et al. UV-A induced oxidative stress is more prominent in naturally pigmented aged human RPE cells compared to non-pigmented human RPE cells independent of zinc treatment. *J Photochem Photobiol B*. 2008;90:113–120.
44. Dontsov AE, Sakina NL, Ostrovsky MA. Loss of melanin by eye retinal pigment epithelium cells is associated with its oxidative destruction in melanolipofuscin granules. *Biochemistry (Mosc)*. 2017;82:916–924.
45. Bazan HE, Bazan NG, Feeney-Burns L, Berman ER. Lipids in human lipofuscin-enriched subcellular fractions of two age populations. Comparison with rod outer segments and neural retina. *Invest Ophthalmol Vis Sci*. 1990;31:1433–1443.
46. Boulton M, Docchio F, Dayhaw-Barker P, Ramponi R, Cubeddu R. Age-related changes in the morphology, absorption and fluorescence of melanosomes and lipofuscin granules of the retinal pigment epithelium. *Vision Res*. 1990;30:1291–1303.
47. Paavo M, Zhao J, Kim HJ, et al. Mutations in GPR143/OA1 and ABCA4 inform interpretations of short-wavelength and near-infrared fundus autofluorescence. *Invest Ophthalmol Vis Sci*. 2018;59:2459–2469.
48. Zhao J, Kim HJ, Sparrow JR. Multimodal fundus imaging of sodium iodate-treated mice informs rpe susceptibility and origins of increased fundus autofluorescence. *Invest Ophthalmol Vis Sci*. 2017;58:2152–2159.
49. Charbel Issa P, Barnard AR, Singh MS, et al. Fundus autofluorescence in the Abca4(-/-) mouse model of Stargardt disease—correlation with accumulation of A2E, retinal function, and histology. *Invest Ophthalmol Vis Sci*. 2013;54:5602–5612.
50. Taubitz T, Fang Y, Biesemeier A, Julien-Schraermeyer S, Schraermeyer U. Age, lipofuscin and melanin oxidation affect fundus near-infrared autofluorescence. *EBioMedicine*. 2019;48:592–604.
51. Shen LL, Sun M, Khetpal S, Grossetta Nardini HK, Del Priore LV. Topographic variation of the growth rate of geographic atrophy in nonexudative age-related macular degeneration: a systematic review and meta-analysis. *Invest Ophthalmol Vis Sci*. 2020;61:2.
52. Zanzottera EC, Messinger JD, Ach T, Smith RT, Curcio CA. Subducted and melanotic cells in advanced age-related macular degeneration are derived from retinal pigment epithelium. *Invest Ophthalmol Vis Sci*. 2015;56:3269–3278.
53. Guidry C, Medeiros NE, Curcio CA. Phenotypic variation of retinal pigment epithelium in age-related macular degeneration. *Invest Ophthalmol Vis Sci*. 2002;43:267–273.
54. Lopez-Rodriguez M, Reina M, Dominguez-Diaz DM, Fajardo V, Villarroel L. (-)-istanbulin a. *Acta Crystallogr Sect E Struct Rep Online*. 2009;65:o2330.
55. Hirasawa M, Noda K, Noda S, et al. Transcriptional factors associated with epithelial-mesenchymal transition in choroidal neovascularization. *Mol Vis*. 2011;17:1222–1230.
56. Kimura K, Orita T, Liu Y, et al. Attenuation of EMT in RPE cells and subretinal fibrosis by an RAR-gamma agonist. *J Mol Med (Berl)*. 2015;93:749–758.
57. Ghosh S, Shang P, Terasaki H, et al. A role for betaA3/A1-crystallin in type 2 EMT of RPE cells occurring in dry

Investigative Ophthalmology & Visual Science

age-related macular degeneration. *Invest Ophthalmol Vis Sci*. 2018;59:AMD104–AMD113.

58. Spaide RF, Curcio CA. Drusen characterization with multimodal imaging. *Retina*. 2010;30:1441–1454.
59. Khan KN, Mahroo OA, Khan RS, et al. Differentiating drusen: Drusen and drusen-like appearances associated with ageing, age-related macular degeneration, inherited eye disease and other pathological processes. *Prog Retin Eye Res*. 2016;53:70–106.
60. Crabb JW, Miyagi M, Gu X, et al. Drusen proteome analysis: an approach to the etiology of age-related macular degeneration. *Proc Natl Acad Sci USA*. 2002;99:14682–14687.
61. Edwards AO, Ritter R, 3rd, Abel KJ, Manning A, Panhuysen C, Farrer LA. Complement factor H polymorphism and age-related macular degeneration. *Science*. 2005;308:421–424.
62. Haines JL, Hauser MA, Schmidt S, et al. Complement factor H variant increases the risk of age-related macular degeneration. *Science*. 2005;308:419–421.
63. Hageman GS, Anderson DH, Johnson LV, et al. A common haplotype in the complement regulatory gene factor H (HF1/CFH) predisposes individuals to age-related macular degeneration. *Proc Natl Acad Sci USA*. 2005;102:7227–7232.
64. Klein RJ, Zeiss C, Chew EY, et al. Complement factor H polymorphism in age-related macular degeneration. *Science*. 2005;308:385–389.
65. Kim YH, He S, Kase S, Kitamura M, Ryan SJ, Hinton DR. Regulated secretion of complement factor H by RPE and its role in RPE migration. *Graefes Arch Clin Exp Ophthalmol*. 2009;247:651–659.
66. Curcio CA, Johnson M, Huang JD, Rudolf M. Aging, age-related macular degeneration, and the response-to-retention of apolipoprotein B-containing lipoproteins. *Prog Retin Eye Res*. 2009;28:393–422.
67. Mullins RF, Schoo DP, Sohn EH, et al. The membrane attack complex in aging human choriocapillaris: relationship to macular degeneration and choroidal thinning. *Am J Pathol*. 2014;184:3142–3153.
68. Katschke KJ, Xi H, Cox C, et al. Classical and alternative complement activation on photoreceptor outer segments drives monocyte-dependent retinal atrophy. *Sci Rep*. 2018;8:7348.
69. Chen L, Messinger JD, Zhang Y, Spaide RF, Freund KB, Curcio CA. Subretinal drusenoid deposit in age-related macular degeneration: histologic insights into initiation, progression to atrophy, and imaging. *Retina*. 2019:1–14.
70. Eamegdool SS, Sitiwin EI, Cioanca AV, Madigan MC. Extracellular matrix and oxidative stress regulate human retinal pigment epithelium growth. *Free Radic Biol Med*. 2020;146:357–371.
71. Greferath U, Guymer RH, Vessey KA, Brassington K, Fletcher EL. Correlation of histologic features with in vivo imaging of reticular pseudodrusen. *Ophthalmology*. 2016;123:1320–1331.
72. McLeod DS, Bhutto I, Edwards MM, Silver RE, Seddon JM, Lutty GA. Distribution and quantification of choroidal macrophages in human eyes with age-related macular degeneration. *Invest Ophthalmol Vis Sci*. 2016;57:5843–5855.